SEGREGATION OF BINARY ALLOYS

COURSE CODE : TP-407

SUBMITTED BY

CLASS ROLL : SN-098-032
EXAM ROLL: 30219
REGISTRATION NUMBER : 2016-014-718
SESSION : 2016-17

DEPARTMENT OF THEORETICAL PHYSICS
UNIVERSITY OF DHAKA

March 24,2022

Contents

List of Figures

1 Abstract

The thermophysical properties of segregating and demixing liquid binary alloys is presented containing the simple methods that are typically operated by physicists, chemists, and metallurgists in general. The different experimental and theoretical data available for such systems are placed together to show a decent knowledge between the experimental results, theoretical processes, and empirical models. The key to learning is the variation that the properties indicate from Raoult's law and the significant modification in the liquid phase as a function of composition, temperature, and pressure. The typical behavior is explained to an outcome of the interplay of the energetic and structural re-adjustment of the constituent elements on mixing. After summarizing the experimental technique and some results, a complete microscopic procedure, based on statistical and hard sphere-like theory, is embarked to elevate the knowledge of the origin of the intriguing processes that are associated with the segregating or phase-separating liquid binary alloys. We terminate by supplying a brief account of the kinetic characteristics of segregation (phase separation) with some deliberate industrial applications.

2 Introduction

Theoreticians have briefed the significance of the mixing properties of binary liquid alloys from both the scientific and the technological points of view. A precise understanding of the mixing properties and phase diagrams of the alloy system is elementary to establish a good arrangement between the experimental results, theoretical approaches, and empirical models for liquid alloys with a miscibility gap. All liquid binary alloys can be grouped into two distinct classes that either exhibit positive deviation(usually called segregating systems) or negative deviation (i.e. short-ranged ordered alloys) from Raoult's law or the additive rule of mixing. If the deviations are considerably large, they may conduct either phase separation or compound formation in the binary system.

There are liquid alloys, however, which do not belong exclusively to any of the above two classes. For instance, the excess Gibbs energy of mixing (G_M^{xs}) for Cd–Na, and Ag–Ge is negative at certain compositions, while positive at other compositions. In liquid alloys such as Au–Bi, Bi–Cd, and Bi–Sb, the

enthalpy of mixing H_M is a positive quantity but G_M^{xs} is negative. Bi–Pb has positive H_M and G_M^{xs} in the solid phase as against the negative values of H_M and G_M^{xs} in the liquid phase[2]. Systems such as Au–Ni and Cr–Mo exhibit immiscibility in the solid phase which is not visible in the interrelated liquid phase. Systems such as Ag–Te show intermetallic phases and large negative H_M values in the liquid phase concurrently with a liquid miscibility gap.

Systems such as Al–Bi, Al–In, Al–Pb, Bi–Ga, Bi–Zn, Cd–Ga, Ga–Pb, Ga–Hg, Pb–Zn, Pb–Si and Cu–Pb, etc, are represented by liquid miscibility gaps and exhibit enormous positive H_M. Their properties in the liquid phase tend to vary markedly as a role of composition (c), temperature (T), and pressure (p). The long-wavelength limit (q→0)of the composition–composition structure factors, S_{cc} (0) diverges as the composition and temperature approach the critical values c $\rightarrow c_c$, and T $\rightarrow T_c$. S_{cc} (0), which can instantly be obtained from thermodynamic functions (either acquired by taking the first composition derivative of the activity or through the second derivative of the Gibbs function), is very useful for establishing the immiscibility and the degree of segregation in binary liquid alloys. Additional thermodynamic, structural, and transport properties are also found to alter anomalously in the area of c_c and T_c.

A provided unary system is expressed by two pairs of independent variables, namely the mechanical degrees of freedom (pressure (p) or volume (Ω)) and the thermal degrees of freedom (temperature (T) or entropy (S)). The preference of independent variables is mostly a concern of free option; yet, there are four possibilities for creating such pairs have one mechanical and one thermal variable, say (S,Ω), (S, p), (T, Ω) and (T, p). These pairs guide to thermodynamic functions such as internal energy E(S,Ω), enthalpy H (S, p), Helmholtz energy F (T, Ω), and Gibbs energy G(T, p), respectively.

The enthalpy, H, merging the internal energy E to the mechanical degrees of freedom (p, Ω) is

$$H = E + p\Omega \tag{1}$$

or in differential form,

$$dH = \delta Q + \Omega dp \tag{2}$$

where

$$\delta Q = dE + pd\Omega$$

The Helmholtz energy, F, relates E to the thermal degrees of freedom (S,T), i.e.

$$F = E - TS \tag{3}$$

or,

$$dF = -SdT - pd\Omega \tag{4}$$

In the case of reversible isothermal and isochoric processes (T , Ω = constant), dF = 0, i.e. F remains invariant. Similarly, the Gibbs function establishes a relation between H and the thermal degrees of freedom, i.e.

$$G = H - TS \tag{5}$$

or

$$dG = -SdT + \Omega dp \tag{6}$$

In the case of a reversible isothermal reaction at constant pressure (T , p = constant), dG = 0, i.e. G remains invariant.

Also, H , F and G can readily be used to obtain the heat capacity C (C_p or C_Ω), entropy, isothermal (χ_T) and adiabatic (χ_S) compressibilities, the volume and the volume expansivity (α_p):

$$C_p = \left(\frac{\partial H}{\partial T}\right)_p = T\left(\frac{\partial S}{\partial T}\right)_p = -T\left(\frac{\partial^2 G}{\partial T^2}\right)_p \tag{7}$$

$$C_\Omega = \left(\frac{\partial E}{\partial T}\right)_\Omega = T\left(\frac{\partial S}{\partial T}\right)_\Omega = -T\left(\frac{\partial^2 F}{\partial T^2}\right)_\Omega \tag{8}$$

$$S = \left(\frac{\partial G}{\partial T}\right)_p = \left(\frac{\partial F}{\partial T}\right)_\Omega \tag{9}$$

$$\Omega = \left(\frac{\partial G}{\partial p}\right)_T \tag{10}$$

$$\chi_T \equiv -\frac{1}{\Omega}\left(\frac{\partial \Omega}{\partial p}\right)_T \tag{11}$$

$$\chi_S \equiv -\frac{1}{\Omega}\left(\frac{\partial \Omega}{\partial p}\right)_S \tag{12}$$

$$\alpha_p \equiv \frac{1}{\Omega}\left(\frac{\partial \Omega}{\partial T}\right)_p \tag{13}$$

At indicator, we furthermore have some important effects from isotherms of liquid–vapor phases which at the critical point must fulfill

$$\left(\frac{\partial p}{\partial \Omega}\right)_{T_c} = \left(\frac{\partial^2 p}{\partial \Omega^2}\right)_{T_c} = 0 \tag{14}$$

At T = T_c , the following physical properties become infinite, i.e.

$$C_p = T\left(\frac{\partial S}{\partial T}\right)_p = \infty \tag{15}$$

$$\alpha_p = \frac{1}{\Omega}\left(\frac{\partial \Omega}{\partial T}\right)_p = \infty \tag{16}$$

$$\chi_T = -\left(\frac{\partial \Omega}{\partial p}\right)_T = \infty \tag{17}$$

For a binary mixture, such as an A–B alloy consisting of c_A moles of component A and c_B moles of component B, rather than guiding to the fundamental values of their function, we define the function of mixing. For example, the Gibbs energy of mixing, G_M , is represented as

$$G_M = G(alloy) - c_A G_A^0 - c_B G_B^0 \tag{18}$$

where G_A^0 and G_B^0 are the Gibbs free energy of the two pure components. Equivalent definitions also exist for HM , SM and other functions.The integral quantities can also be divided into the partial quantities, i.e.

$$G_M = c_A \overline{G}_{M,A} + c_B \overline{G}_{M,B} \tag{19}$$

with

$$\overline{G}_{M,i} = RTlna_i \qquad (\text{ i= A,B })$$

where $\overline{G}_{M,i}$ are the partial Gibbs energies and a_i are the thermodynamic activities of the component i. G_M defines the stability of the phases in a binary mixture. The curves describing G_M against c deviation can, in general, have a shape like either curve a or curve b as displayed in figure 1.[3] For G_M as in curve a, the homogeneous solution is stable at all values of c at T_1 ; if not other phases (i.e. intermediate phases) in the system display more negative G_M values.

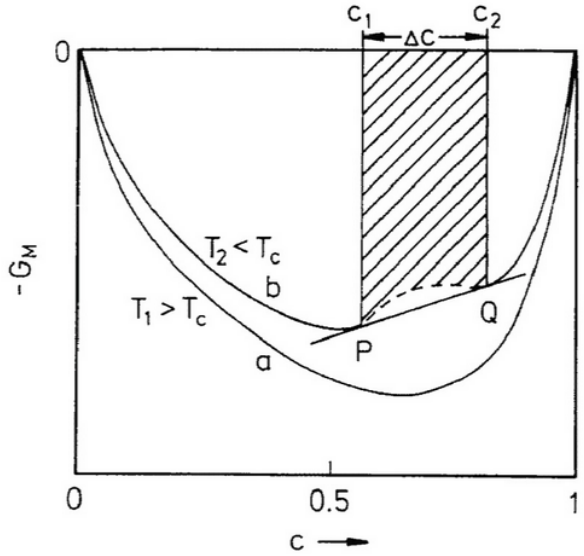

Figure 1: A schematic diagram symbolizing the Gibbs energy of mixing at constant T plotted against concentration. Curve a, complete mixing ($T_1 < T_c$). Curve b, incomplete mixing ($T_2 < T_c$), Δc represents the miscibility gap at T_2 .

For curve b, the homogeneous solution is varying in the composition range Δc, because G_M can be reduced if the mixture separates into two phases. The composition of these phases is provided by the points of contact P and Q of the common tangent line to the G_M(c) curve. The reduced G_M values of these two phases are given by this line. Within the composition range Δc only the portions of the two phases change if the total composition of the alloy modifications. At P(c_1) and Q(c_2) the partial Gibbs energies of the components of both diverged phases are equivalent,

$$\overline{G}_{M,i}(c_1) = \overline{G}_{M,i}(c_2) \qquad (\text{ i= A,B })$$

Hence P and Q indicate the limit of thermodynamic equilibrium. G_M diverts as a function of temperature from a concave to a convex surface for Δc at the spinodal. The points of inflection in the curves define the spinodal line. The critical composition and the critical temperature are determined from the conditions at T = T_c

$$\left(\frac{d^2G_M}{dc^2}\right)_{c=c_c} = 0 \tag{20}$$

$$\left(\frac{d^3G_M}{dc^3}\right)_{c=c_c} = 0 \tag{21}$$

At this step, it should be pointed out that the long-wavelength limit (q $\rightarrow$ 0) of the structure factor S_{cc}(q) which is well known as the concentration fluctuation, $S_{cc}(0)$, is also correlated to the thermodynamic function, i.e

$$S_{cc}(0) = RT\left(\frac{d^2G_M}{dc^2}\right)^{-1}_{T,P} \tag{22}$$

As $c \rightarrow c_c$ and $T \rightarrow T_c$,one sees that

$$S_{cc}(0) \rightarrow \infty \tag{23}$$

Thus, a phase separation in a binary mixture is signaled by a strong enhancement of the concentration fluctuations. The ideal solution behavior (HM = 0) of a binary mixture is presented by

$$G_M^{id} = RT(c_A\ lnc_A + c_B\ lnc_B). \tag{24}$$

The distinctions in the thermodynamic behavior of a real binary solution and an ideal solution are represented by the excess quantities, i.e.

$$G_M^{xs} = G_M - G_M^{id} \tag{25}$$

or using equation (5)

$$G_M^{xs} = H_M - TS_M^{xs} \tag{26}$$

with

$$S_M^{xs} = S_M + R(c_A\ lnc_A + c_B\ lnc_B) \tag{27}$$

This report is categorized in the following ways: section-3, Observable indicators; section-4, Optimization of thermodynamic data; section-5, Electronic theory of mixing; section-6, Hard-sphere like theory for segregation; section 7, summary; section 8, References.

3 Observable indicators

3.1 Segregating liquid alloys

From the point of view of interatomic interactions, a binary alloy is either (i) an ordered alloy, where unlike atoms are chosen as nearest neighbors over like atoms, or (ii) a segregated alloy, where like atoms are chosen to pairs as nearest neighbors over unlike atoms. Unfortunately, there is no direct way to distinguish the constituent atoms and hence the identification of a nearest-neighbor pair of atoms is challenging. In this case either the structural data or the experimental thermodynamic functions (such as activity, the heat of mixing, excess Gibbs energy of mixing, excess heat capacity, etc) or other thermophysical data (such as viscosity, diffusivity, density, surface tension, electrical resistivity, etc) are supposed to extract information associated with interatomic interactions. Some of the empirical criteria as well as microscopic parameters which are used to identify segregated alloys are summarized below.
(a) Alloys displaying positive deviations from Raoult's law.
(b) The heat of formation and the excess Gibbs energy of mixing are positive.
(c) The concentration fluctuation in the long-wavelength limit ($S_{cc}(0)$) is greater than the ideal value.

Table 1 provides a list of G_M^{xs} , H_M and S_M^{xs} at the equiatomic composition of segregating liquid alloys which are arranged according to the type of their phase equilibria. Of these Bi– Zn, Pb–Zn, Cu–Pb, Cd–Ga, Al–Bi, Al–In, Al–Pb, etc, exhibit liquid immiscibility. G_M^{xs} and H_M are comparatively large positive quantities. For these alloys only a few experimental heat capacity data are available . The data, in general, show a decrease in Cp with increasing temperature. The energetic and structural effects in the solution phase can be more directly seen by the excess heat capacity ΔC_pvalues:

$$\Delta C_p = C_p(c) - c_A \; C_{p,A} - c_B \; C_{p,B} \tag{28}$$

ΔC_p are positive and indicate maximum values near to T_c and c_c .

Table 1: Thermodynamic properties of liquid binary alloys at equiatomic composition displaying segregation. The values are from Ref.[4] [(i) Hultgren et al 1973, (iii) Yu 1994]

Alloys	Ref.	T (K)	G_M^{xs}/RT	H_M/RT	S_M^{xs}/R
Al–Bi	(i)	900	0.814	0.823	0.09
Al–In		1150	0.54	0.49	-0.05
Al–Pb		1700	0.527	0.847	0.32
Bi–Ga	(ii)	550	0.493	0.433	-0.06
Bi–Zn		880	0.36	0.60	0.24

Since the pioneering work by Hume-Rothery and his coworkers (Ref.[5] Hume- Rothery and Raynor 1954), a substantial effort has been assembled to identify the factors impacting the alloying behavior of liquid metallic mixtures, such as the difference in atomic sizes, valence differences, electronegativity differences, etc. For the sake of a brief perusal, we enroll the basic physical, thermochemical and structural properties of pure liquid metals (near the melting points) in table 1.1 which are the components of the binary mixture of table 1. These properties are also useful for further discussions. At this step, it is not possible to single out any individual elemental properties which might be held reliable for demixing of liquid alloys. Yet, the practical analyses recommend that quantities such as atomic size, the heat of vaporization, and electronegativity together hold the key to the knowledge of the segregation or order in a liquid alloy.

3.2 Thermodynamic properties

Some of the thermodynamic properties of equiatomic segregating liquid alloys are tabulated in table 1. Here we intend to discuss briefly the salient features of the various experimental techniques and the specific results that exist as a function of concentration and temperature. The experimental methods used to obtain reliable thermodynamic data at constant pressure as a function of composition and temperature are briefly summarized.The entropy of formation S_M of an alloy can only be defined directly from C_p(c, T) data

$$S_M(c,T) = \int_0^T \frac{\Delta C_p(c,T)}{T} dT \tag{29}$$

Table -1.1 Some physical, chemical and structural properties of liquid metals (near melting temperature) are associated with the formation of segregating type metallic mixtures. m, atomic weight (1u = 1.66×10^{-27} kg); T_m , melting point; Ω, volume; ΔH_m , enthalpy of melting; ΔH_v , enthalpy of evaporation; ΔS_m , entropy of melting; ΔS_v , entropy of vaporization; r_1 nearest-neighbour distance; Z, first shell coordination; Γ, surface tension; x, Pauling electronegativity value. (i) After Iida and Guthrie (1988), (ii) after Waseda (1980); (iii) after Pauling (1960)

Metals	$m^{(i)}$ (u)	$T_m^{(i)}$ (K)	$\Omega^{(i)}$ $(10^{-6}m^3)gmol^{-1}$	$\Delta H_m^{(i)}$ $(kJmol^{-1})$	$\Delta H_v^{(i)}$ $(kJmol^{-1})$	$\Delta S_m^{(i)}$	$\Delta S_v^{(i)}$	$r_1^{(ii)}$	$Z^{(ii)}$	$\Gamma^{(i)}$	$(x)^{(iii)}$
Al	26.98154	933.35	11.6	10.46	291	11.2	104	2.82	11.5	914	1.5
Bi	208.9804	544.1±0.05	20.80	10.88	179	20.0	97.4	3.38	8.8	378	1.9
Cd	112.41	594.05	14.00	6.40	100	10.8	96.2	3.11	10.3	570	1.7
Ga	69.72	302.93±0.005	11.40	5.59	270	18.4	100	2.82	10.4	718	1.6
In	114.82	429.55	16.3	3.26	232	7.58	98.9	3.23	11.6	556	1.7
Pb	207.2	600.55	19.42	4.81	178	8.02	88.0	3.33	10.9	458	1.8
Zn	65.38	692.62	9.94	7.28	114	10.5	96.6	2.68	10.5	782	1.6

To obtain S_M according to equations (28) and (29) the C_p values of the components and the alloy have to be known down to 0 K as well as the entropy of transformations that take place below T . There are several problems. At first, the differences between the Cp valuesof the mechanical mixture and the alloy are small and one has to know the C_p values to high accuracy to get reliable results for S_M . Equation (29) uses likewise to ordered crystalline substances in the solid-state only. Alloys are occasionally disordered at room temperature and remain so down to 0 K. S_M values of a liquid alloy cannot be acquired from equation (29) because the C_p values of the undercooled

liquid state for the components and the alloys have to be verified specifically. Since for multicomponent systems, the reference state is the mechanical mixture of the pure components in the same state as the solution, the entropy of formation of solid and liquid alloys are, hence, typically confined from experimentally obtained G_M(c, T) and H_M(c, T) values according to equation (5).

3.3 Calometric measurements

The enthalpy of formation H_M, their partial values $\overline{H}_{M,i}$ and the heat capacity of liquid alloys can be directly specified by calorimetric methods. An isoperibolic type of calorimeter which operates at constant T is particularly appropriate for calculating H_M and $\overline{H}_{M,i}$ of a liquid alloy as a function of composition at constant T directly.The H_M values acquired for liquid In–Cd alloys at 628 K are shown in figure 2 as an example.

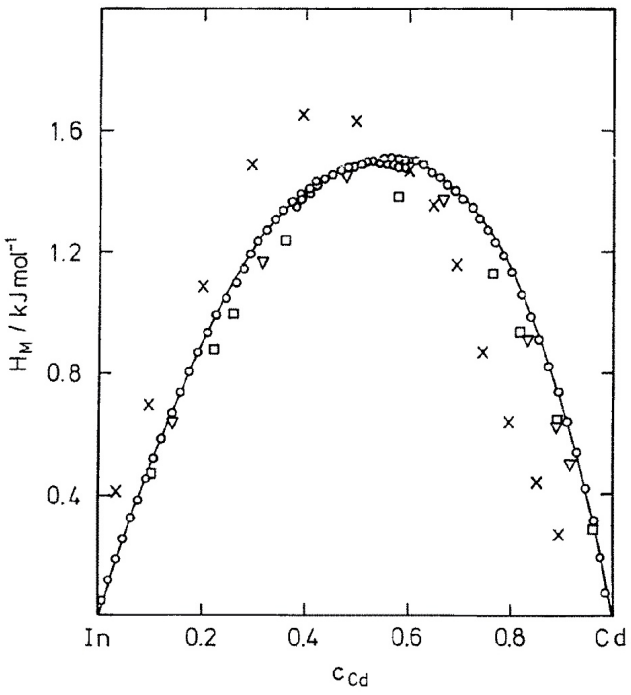

Figure 2: Enthalpy of mixing of liquid Cd–In alloys.

If the modification in concentration Δc_A is small for each successive step (i.e. < 1 $at.\%$), $dH_M(c)/dc$ can be confined in a suitable approximation by

$$\frac{dH_M(c)}{dc_A}\left(c_A + \frac{\Delta c_A}{2}\right) = \frac{H_M(c_A + \Delta c_A) - H_M(c_A)}{\Delta c_A} \tag{30}$$

The partial values of a multi-component system are obtained by

$$\overline{H}_{M,i} = H_M + \sum_{j=2}^{r}(\delta_{ij} - c_j)\frac{\partial H_M(c)}{\partial c_j} \tag{31}$$

with $\delta_{ij} = 0$ for $i \neq j$ and $\delta_{ij} = 1$ for $i = j$. r is the number of components. Figure 3 shows the experimentally determined slope dH_M/dc_{C_d} of liquid In–Cd alloys at 628 K. These results undoubtedly show that small deviations from a standard solution behaviour ($H_M(c) = Ac_Ac_B$) exist.[3]

The heat capacity of liquid alloys can be specified directly by adiabatic calorimetry. Adiabatic calorimetry applies to calculate the heat input ΔQ to a sample and the associated temperature increase ΔT. Heat losses have to be minimized by proper surroundings to approximate an adiabatic chamber for the sample. The specific heat over the temperature increase is given by

$$C_p = \frac{\Delta Q}{m\Delta T} \tag{32}$$

where m is the mass of the sample.

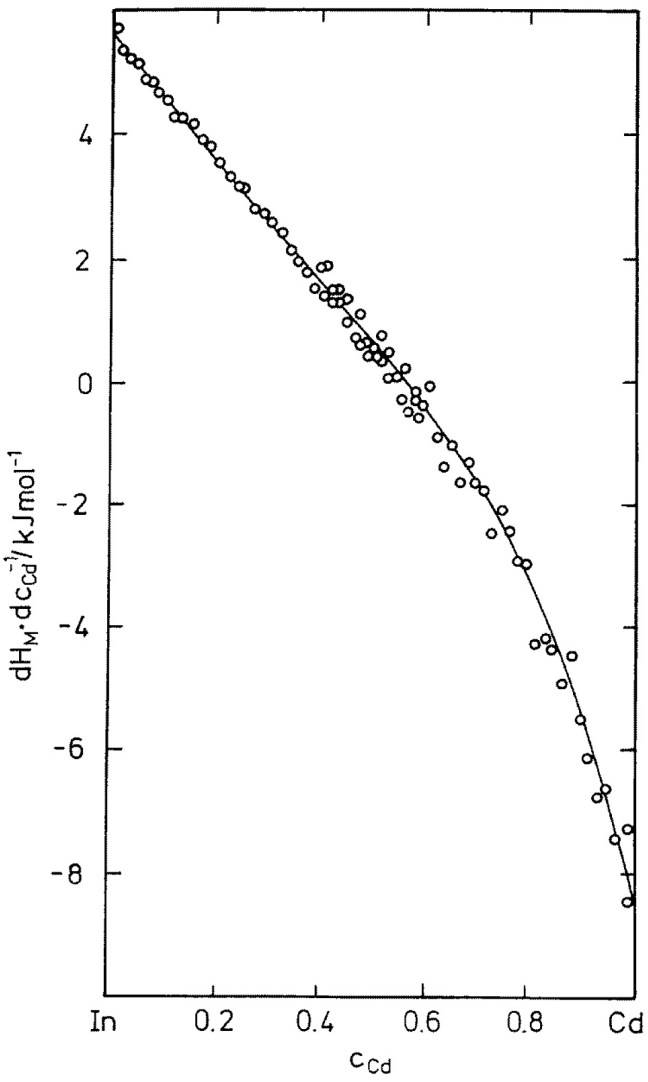

Figure 3: Calorimetrically determined slope of the enthalpy of mixing of liquid Cd–In alloy at 628 K (after Predel and Oehme 1977).Ref.[1]

4 Optimization of thermodynamic data

Thermodynamic calculations of phase equilibria are widely used to check the consistency of data got from different experimental measurements (phase diagram data, results of calorimetry). Model descriptions using statistical thermodynamics or polynomial expressions are used to represent the thermodynamic properties of all phases applied.The adjustable coefficients are determined by a weighted least-squares method (Ref.[6] Lukas and Fries 1992). The essential feature of this procedure is to obtain a uniform set of model parameters in an analytical representation. This helps one to gather into temperature and concentration regions where the direct experimental determination is difficult. It also allows one to estimate safely the thermodynamic data of metastable phases. Finally, the thermodynamic description of multicomponent systems can be gathered from those already calculated for their subsystems. The strategy of such a critical assessment will be demonstrated for the demixing Al–In, Al–Pb, Cd–Ga, and Bi–Zn systems.

4.1 The Al–In System

The H_M values near the equiatomic composition received by Ref.[7] Predel and Sandig (1969a) are about 50% more enormous than the values determined by Girard (1985) Ref.[8]and Sommer et al (1993) .The alloy samples, each of about 0.5 g, were included in a closed graphite crucible which was encapsulated under argon in a quartz glass ampule. The quartz glass ampules were mechanically vibrated at about 1200 K to ensure a homogeneous liquid alloy before the DTA experiment on cooling was formed to obtain the binodal. The critical temperature amounted to 1112 K.
In the background of this information, the optimization is performed. The major task is to characterize the thermodynamic properties as a power-series law whose coefficients (say, A, B, C, D, . . .) are determined by the least-squares method. The heat capacity can be expressed as

$$C_p = -C - 2DT - 2ET^{-2} - .... \tag{33}$$

The enthalpy and energy is given by

$$H = H(T_0) + \int_0^T C_p dT \tag{34}$$

or
$H = A - CT - DT^2 + 2ET^{-1} - ....$
and

$$S = S(T_0) + \int_0^T \frac{C_p}{T} dT \tag{35}$$

or
$S = -B - C(1 + lnT) - 2DT + ET^{-2} - ...$

Using equation (5), the T dependence of the Gibbs energy may be written as

$$G = A + BT + CTlnT + DT^2 + ET^{-1} + ... \tag{36}$$

The composition dependency of the excess Gibbs energy of mixing is given by a polynomial such as the Redlich–Kister polynomial (Redlich and Kister 1948):

$$G_M^{xs}(c,T) = c_A c_B \sum_{l=0}^{m} K_l(T)(c_A - c_B)^l \tag{37}$$

with $K_l(T) = A_l + B_l T + C_l T lnT + D_l T^2 + ...$ The coefficients Kl have the same temperature dependence as G in equation (37). The partial quantities are given by

$$\overline{G}_A^{xs}(c,T) = c_B^2 \sum_{l=0}^{m} K_l(T)[(1+2l)c_A - c_B](c_A - c_B)^{l-1} \tag{38}$$

$$\overline{G}_B^{xs}(c,T) = c_A^2 \sum_{l=0}^{m} K_l(T)[c_A - (1+2l)c_B](c_A - c_B)^{l-1} \tag{39}$$

The pure solid elements Al and In in their stable form at 298.15 K and 1bar were chosen as the reference state of the system. The Gibbs energies of the elements as functions of the

Table 2: Optimized coefficient set of G_M^{xs} (equation (37)) for liquid Al–In alloys

l	A_l $(Jmol^{-1})$	B_l $(Jmol^{-1}K^{-1})$
0	18641.14	1.74886
1	558.36	1.14350
2	10692.88	7.47862
3	1346.56	0

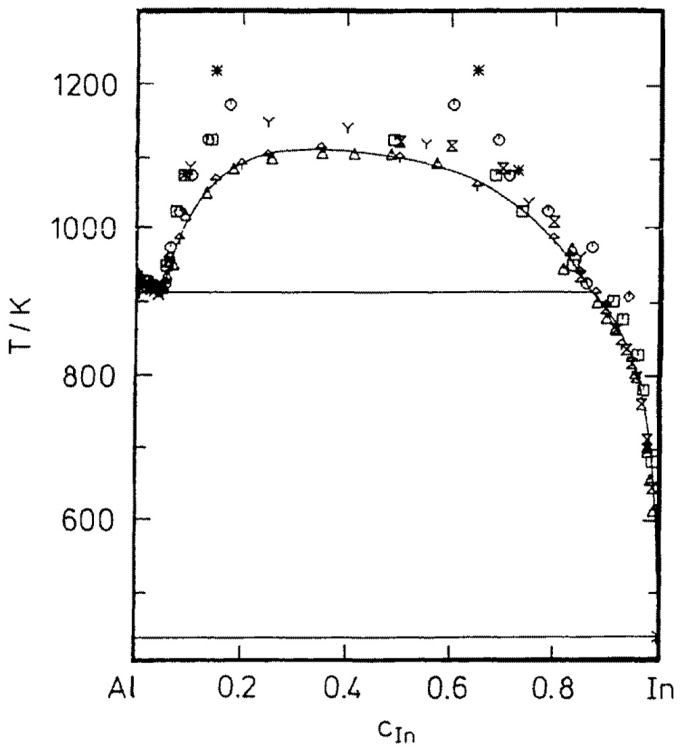

Figure 4: calculated phase diagram (continuous curve) using the coefficient set given in table 2.

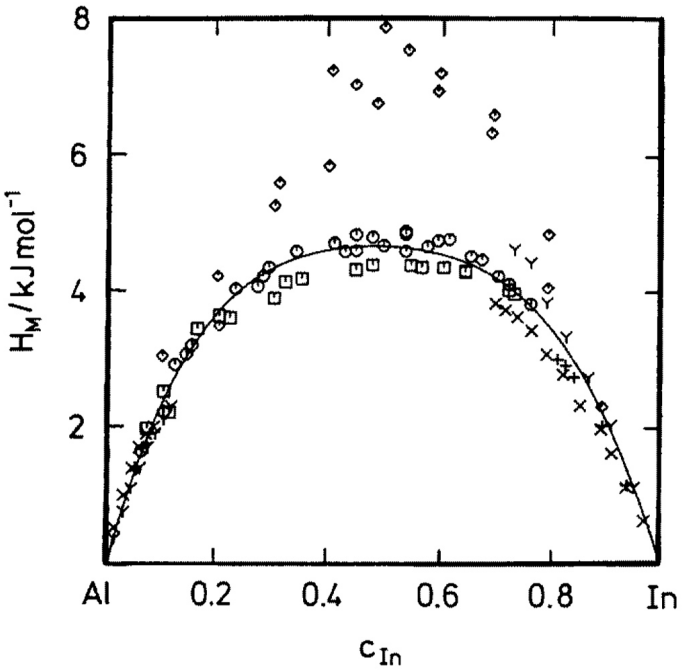

Figure 5: Calculated enthalpy of mixing (continuous curve) using the coefficient set given in table 2.

temperature were compiled by Dinsdale (1991) and no solid solubility was considered. The excess Gibbs energy of the liquid alloy is represented by equation (37). The optimized coefficients are given in table (3) and the phase diagram in figure (4).

4.2 The Al–Pb system.

The experimental results on Al–Pb imply a vast liquid miscibility gap due to the strong segregation tendency of the components. The solubility of lead in solid aluminum is less than 0.025 at.% Pb at the monotectic temperature of around 932 K. The solubility of Al in Pb is basically negligible. A lot of phase diagram data are available at temperatures below 1200 K in narrow terminal sides below 3 at.% Pb and above 90 at.% Pb. These data are in acceptable agreement as the evaluation of McAlister (1984) has shown. McAlister has

Table 3: Optimized coefficient set of G_M^{xs} (equation (37)) for liquid Al–Pb alloys

l	A_l $(Jmol^{-1})$	B_l $(Jmol^{-1}K^{-1})$
0	47993.6	-10.71995
1	14407.33	-6.65287
2	4742.36	-0.72034

evaluated a critical temperature of 1839 K at 44.8 at.% Pb. This T_c value is considerably higher than the value specified by Predel and Sandig (1969b) operating DTA. Yu et al (1996) have redetermined the binodal using a new isopiestic method (Wang et al 1993). There are only a few thermodynamic data available, due to the experimental difficulties associated with the small solubility of liquid aluminum and lead, and the high vapor pressure of lead at high temperatures.

The phase equilibria are calculated by choosing the pure elements in their stable state at 298.15 K and 1 bar as the reference state of the system. Their Gibbs energies are given by Dinsdale (1991). The excess Gibbs energy of the liquid alloy is represented by equation (37). The calculation carried out by Yu et al (1996) takes into account the elemental thermodynamic data due to Dinsdale (1991), the phase diagram data at temperatures above 1500 K that are obtained with the isopiestic method, and the data of Predel and Sandig (1969b) on the Pb-rich side below 1600 K. The resulting optimized set of parameters are given in table (4). The entire phase diagram is given in figure (6).

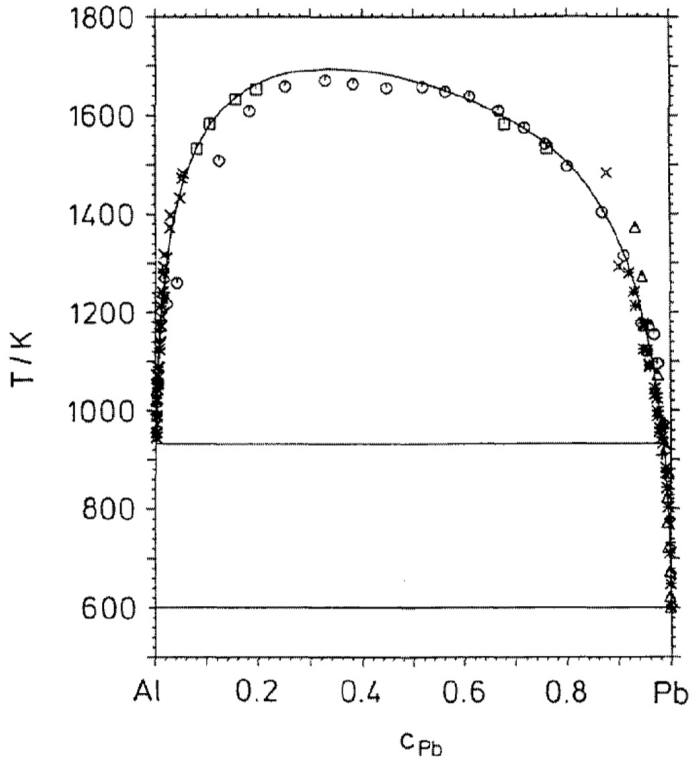

Figure 6: Calculated phase diagram (continuous curve) using the coefficient set given in table 3.

4.3 The Cd–Ga system.

The Cd–Ga system shows a flat liquid miscibility gap with $T_c = 568$ K and $c^c_{Ga} = 39.9$ at.% (see figure 12). The pure solid elements in their stable state at 298.15 K and 1 bar were chosen as the reference state of the system and no solid solubility of the components was considered. The Gibbs energies of the pure elements were taken from Dinsdale (1991). The excess Gibbs energy of the liquid alloy was expressed with equation (37) and the resulting coefficient set of the optimization is given in table 4.

The calculated phase equilibria are shown in figure 7. The experimentally determined temperature dependence of HM (see figure 8) and the cadmium

Table 4: Optimized coefficient set of G_M^{xs} (equation (37)) for liquid Cd–Ga alloys

l	A_l $(Jmol^{-1})$	B_l $(Jmol^{-1}K^{-1})$	C_l $(Jmol^{-1}K^{-1})$	D_l $(Jmol^{-1}K^{-2})$
0	-18447.76	483.09573	-71.723197	0.041784
1	-3189.49	38.38390	-5.153091	0
2	3054.07	-2.49129	0	0

activity data of the liquid alloy (see figure 9) are consistent with the calculation.

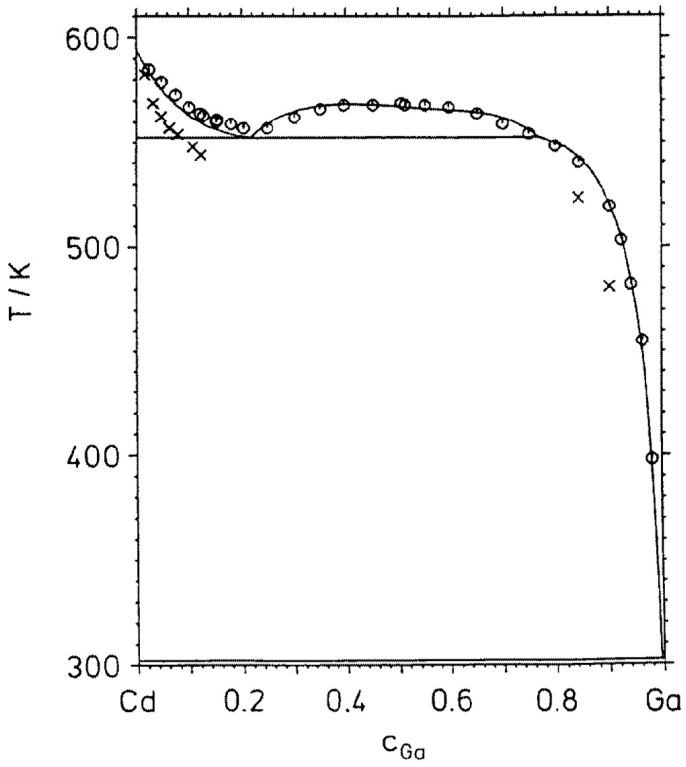

Figure 7: Calculated phase diagram (continuous curve) using the coefficient set given in table 4.

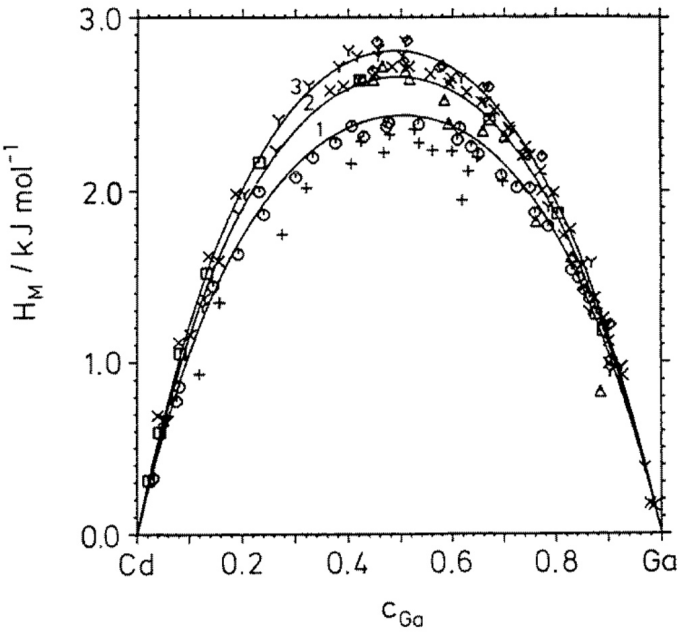

Figure 8: Calculated (continuous curve) enthalpy of mixing at different temperatures (1, 609 K; 2, 656 K; 3,695 K) using the coefficient set given in table 4.

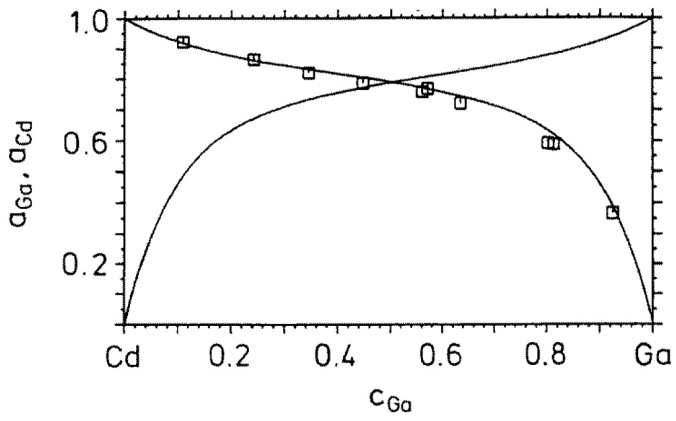

Figure 9: Calculated (continuous curve) activities at 742 K using the coefficient set given in table 4.

4.4 The Bi–Zn system.

The liquid zinc-rich Bi–Zn alloys exhibit a comprehensive miscibility gap with $T_c = 863.8$ K, $c^c_{Zn} = 87$ at.% (see figure 10). At the monotectic temperature of 688.5 K hcp zinc and two liquid alloys with the composition 38.6 and 99.1 at.% Zn, respectively, are in equilibrium. These results are obtained from an optimization calculation by the least-squares method (Lukas et al 1977). Preliminary results are given by Wang et al (1993). No solid solubility of the components was assumed. The thermodynamic data for the elements were assumed from Dinsdale (1991). The resulting set of coefficients describing G^{xs}_M (equation (37)) of the liquid alloys is given in table 5. A comparison between calculated H_M and activity values and the experimental data are shown in figures 11 and 12.

Table 5: Optimized coefficient set of G_M^{xs} (equation (37)) for liquid Cd–Ga alloys

l	A_l $(Jmol^{-1})$	B_l $(Jmol^{-1}K^{-1})$
0	17633.89	-7.91451
1	-6607.32	1.34247
2	3873.47	-1.08723
3	0	0
4	7975.68	-9.81903
5	-4553.59	0

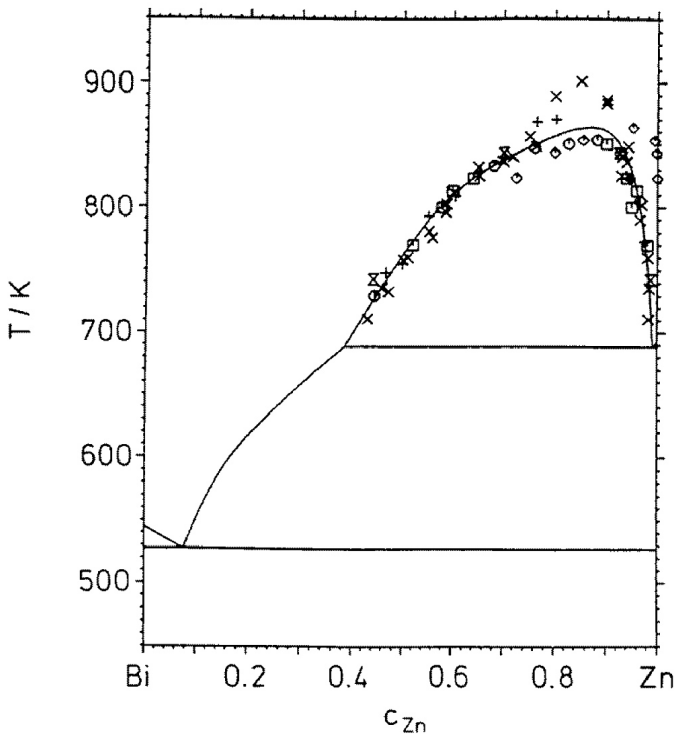

Figure 10: Calculated (continuous curve) phase diagram using the coefficient set given in table 5.

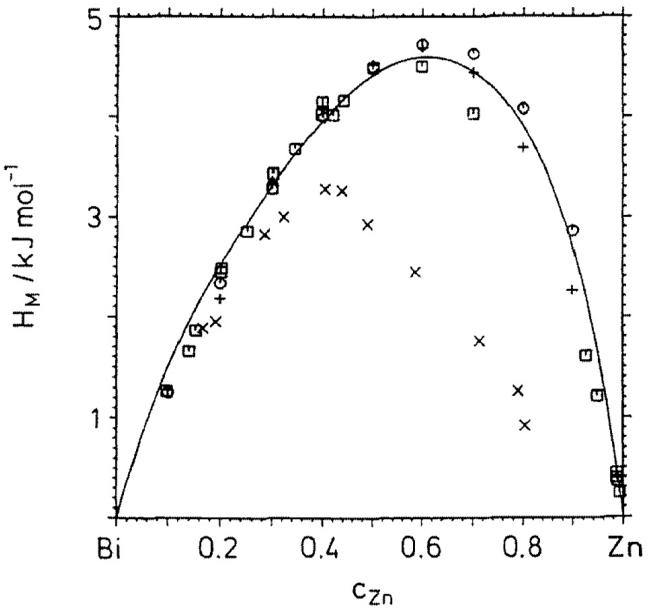

Figure 11: Calculated (continuous curve) enthalpy of mixing of liquid Bi–Zn alloys using the coefficient set given in table 5.

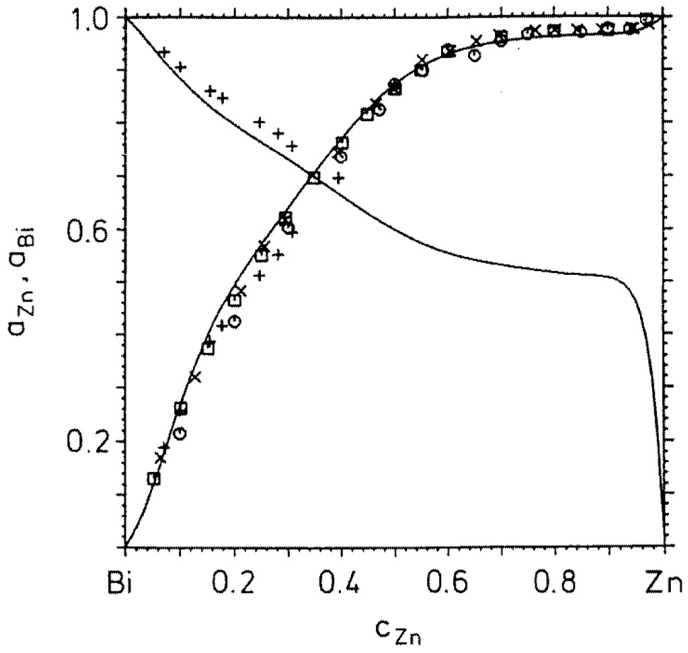

Figure 12: Calculated (continuous curve) activity of liquid Bi–Zn alloy at 873 K using the coefficient set given in table 5.

5 Electronic theory of mixing

The electronic theory in a major way provides a platform where the energies and structure of a liquid metallic system can be merged (Harrison 1966, Heine 1970, Stroud and Ashcroft 1972) to remove absorbing physical properties of the system. There is no exact difference between nearly-free-electron (NFE) and non-NFE alloys. Yet, the physical properties of the two classes of alloys that are dependent on the number of valence electrons (electrical resistivity, thermoelectric power, Hall coefficient, magnetic susceptibility, knight shift) are usually extremely distinguishable. Also, the valence and the electronegativity differences are smaller in NFE and larger for the non-NFE systems. The work on phase-separating liquid alloys based on electronic theory is insufficient, although safe to apply to simple segregating liquid alloys without incurring noticeable error. The value of the theory stands from the fact that

it is free from any assumptions and, as such, there should not be an adaptable parameter. One can, at least, gather some first-hand information on the basic interatomic forces (φ_{ij}) which are directly related to the energy parameter (ω) occurring in previous sections. In addition, it helps to identify the volume and the structure-dependent contributions to the energy of the process of mixing.

5.1 Pseudopotential perturbation scheme

The NFE binary alloys can be considered to consist of a system of ions and valence electrons. The fundamental Hamiltonian which explains the system is of the form

$$H = H_e + H_i + H_{ei} \tag{40}$$

with

$$H_e = T_{elec} + \frac{1}{2}\sum_{i=j}\frac{e^2}{|\overline{r_i} - \overline{r_j}|} - H' \tag{41}$$

$$H_i = T_{ions} + \frac{1}{2}\sum_{i=j}\frac{z_i z_j e^2}{|R_i - R_j|} - H' \tag{42}$$

$$H_{ei} = \sum_{i,j} V(\overline{r_i} - \overline{R_j}) + 2H' \tag{43}$$

(e, electron; i, ion; and ei, electron-ion). T stands for kinetic energy,$\overline{r}$and are electronic and atomic positions and z is the valency. It is assumed that electrons and ions always interact among themselves Coulombically. The electron-ion interaction V will be accepted as a pseudopotential. Within an acceptable uncertainty, the ions are likely to drive much more slowly than the electrons, and, hence, the various contributions thus deriving from (40) can be treated individually. H' is the self-energy of a uniform charge distribution that is inserted to maintain the net potential energy expressions finitely. Referring to Hamiltonian (40), the internal energy, E, can be described in atomic units (for a detailed description see Ashcroft and Stroud (1978)),

$$E = E_e + E_i + (E_{ei}^I + E_{ei}^{II}) \tag{44}$$

with

$$E_e = \overline{z}\left[\frac{3}{10}K_F^2 - \frac{3}{4\pi}K_F - 0.0474 - 0.0155lnK_F - \frac{1}{2}\left(\frac{\pi k_B}{K_F}\right)^2 T^2\right] \quad (45)$$

$$E_i = \frac{3}{2}k_B T + \frac{1}{\pi}\sum_{i,j}^{A,B} z_i z_j \left(c_i c_j\right)^{\frac{1}{2}} \int_0^\infty \left(S_{ij}(q) - \delta_{ij}\right) dq \quad (46)$$

$$E_{ei}^{II} = \lim_{q\to 0} \overline{z}\varrho \left[\sum_i c_i V_i(q) + \frac{4\pi\overline{z}}{q^2}\right] \quad (47)$$

$$E_{ei}^{II} = \frac{1}{16\pi^3}\int_0^\infty q^4 dq \sum_{ij} V_i(q)V_j(q)\left(c_i c_j\right)^{\frac{1}{2}} S_{ij}(q)\left(\frac{1}{\epsilon^*(q)} - 1\right) \quad (48)$$

where $K_F = \left(3\pi^2\overline{z}\varrho\right)^{\frac{1}{3}}$, $\overline{z}\varrho = z_A\varrho_A + z_B\varrho_B$ and $\overline{z} = c_A z_A + c_B z_B$; z_A and z_B are valencies, ϱ_A and ϱ_B are the number densities of the ion species and $\varrho = \varrho_A + \varrho_B$. E_{ei}^I and E_{ei}^{II} are due to the electron-ion interaction specified through first and second-order pseudopotential perturbation theory, respectively. $V(q)$ is the Fourier transform of the bare ion pseudopotential and is named the form factor. $\epsilon^*(q)$ is the altered Hartree dielectric function which brings into account the interaction of the conduction electrons.

S_{ij} are the partial structure factors that take care of the arrangement of ions in the system. For a hard-sphere system, S_{ij} can readily be calculated following the work by Ashcroft and Langreth (1967). The necessary inputs are the diameters of the hard spheres (σ) whose preference has always been a matter of interest (see, for example, Faber 1972, Shimoji 1977). However, to make the present scheme internally consistent, we suggest that σ should be specified in the variational thermodynamic purpose equipping minimum free energy for the system, i.e.

$$\left(\frac{\partial F}{\partial \sigma}\right)_{\Omega,T} = 0 \quad (49)$$

with

$$F = E - TS_{hs} \quad (50)$$

where S_{hs} is the entropy of the hard sphere mixture which consists of

$$S_{hs} = S_{id} + S_{gas} + S_{\eta} + S_{\sigma} \tag{51}$$

where S_{id} is the ideal entropy of mixing, S_{gas} is the ideal gas entropy, S_{η} is the contribution which depends only on packing density and S_{σ} denotes the entropy contribution due to mismatch of the hard sphere diameters σ_1 and σ_2 .

The operating expressions for these quantities may be described as (Mansoori et al 1971, Umar et al 1974):

$$S_{id} = -k_B \sum_{i=1}^{2} c_i ln c_i \tag{52}$$

$$S_{gas} = \frac{5}{2}k_B + k_B ln \left[\frac{1}{\varrho} \left(\frac{m_A^{c_A} m_B^{c_B} k_B T}{2\pi\hbar^2} \right)^{\frac{3}{2}} \right] \tag{53}$$

$$S_{\eta} = k_B ln b + 1.5 k_B (1 - b^2) \tag{54}$$

$$S_{\sigma} = \frac{\pi c_A c_B \varrho (\sigma_A - \sigma_B)^2 b^2}{24} [12(\sigma_A + \sigma_B) - \pi\varrho(c_A\sigma_A^4 + c_B\sigma_B^4)] \tag{55}$$

with $b = (1 - \eta)^{-1}$. The first two terms in equation (51) are structure-independent terms and depend only on concentration c, atomic mass m, and atomic volume Ω. The last two terms are structure-dependent contributions due to the existence of the packing fraction, $\eta (= (\pi\varrho/6)(c_A\sigma_A^3 + c_B\sigma_B^3))$ and the hard-sphere diameter σ_i .

The present method helps to specify the energy contributions from the constituent species such as electrons and ions. Also, it helps us to separate the energies of the formation of a binary alloy due to just volume-dependent and structure-dependent contributions, respectively.

The Hamiltonian as expressed in equation (40) allows (see, for example, Ashcroft and Stroud 1978, Young 1992) one to estimate the effective interatomic potentials as,

$$\phi_{ij}(r) = \frac{z_i z_j e^2}{r} + \frac{1}{(2\pi)^3} \int \frac{q^2}{4\pi e^2} V_i(q) V_j(q) \left[\frac{1}{\epsilon^*(q)} - 1 \right] \frac{\sin qr}{qr} 4\pi q^2 dq \tag{56}$$

$\phi_{ij}(r)$ can readily be coupled to the radial distribution function, $g_{ij}(r)$.

6 Hard-sphere like theory for segregation

6.1 Hard sphere mixture under the Percus–Yevick approximation

The stability of binary alloys by treating them as a mixture of hard spheres, i.e.

$$\begin{aligned} \phi(r) &= \infty && \text{(for } r < 0\text{)} \\ \phi(r) &= 0 && \text{(for } r > 0\text{)} \end{aligned} \tag{57}$$

Although the potential (equation (57)) is devoid of an attractive interaction, it equips a useful insight into which forms the effective short-range repulsive interaction governs the geometrical packing at metallic densities. The quantity of major significance is the direct correlation function, $C_{ij}(r)$, which is connected to $g_{ij}(r)$ and $\phi_{ij}(r)$ via the Percus–Yevick (PY) equation (Percus and Yevick 1958):

$$C_{ij}(r) = g_{ij}(r)\left(1 - exp\frac{\phi_{ij}}{k_B T}\right) \qquad \text{(i , j = A , B)}$$

The analytical solution of the PY equation for a mixture of hard spheres was obtained by Lebowitz (see Lebowitz 1964, Lebowitz and Rowlinson 1964). As regards the hard-core interactions in the mixture, these authors considered additive hard-sphere mixtures, i.e

$$\sigma_{AB} = \frac{\sigma_{AA} + \sigma_{BB}}{2} \tag{58}$$

The free energy per particle of the mixture can be written as

$$F_{hs} = c_A\mu_A + c_B\mu_B - P_{hs}\Omega \tag{59}$$

$$G_{hs} = c_A\mu_A + c_B\mu_B \tag{60}$$

Here the μ_i are the chemical potentials of the components and P_{hs} is the pressure:

$$\frac{\mu_i}{k_BT} = ln\left[\Omega_i^{-1}\left(\frac{2\pi\overline{h}^2}{m_ik_BT}\right)^{(}3/2)\right] - ln(1-\eta) + \frac{3X\sigma_{ij}}{(1-\eta)} + \frac{3}{2}\left[\frac{3X^2}{(1-\eta)^2} + \frac{2Y}{(1-\eta)}\right]\sigma_{ii}^2 + \frac{\pi P_{hs}\sigma_{ii}^3}{6k_BT} \tag{61}$$

and

$$\frac{P_{hs}}{k_BT} = \frac{\Omega^{-1}(1+\eta+\eta^2) - \frac{1}{2}\pi\Omega_A^{-1}\Omega_B^{-1}(\sigma_{AA}-\sigma_{BB})^2(\sigma_{AA}+\sigma_{BB}+\sigma_{AA}\sigma_{BB}X)}{(1-\eta)^3} \tag{62}$$

where

$$X = \frac{\pi}{6\Omega}\sum_i c_i\sigma_{ii}^2 \tag{63}$$

$$Y = \frac{\pi}{6\Omega}\sum_i c_i\sigma_{ii} \tag{64}$$

$$\eta = \frac{\pi}{6\Omega}\sum_i c_i\sigma_{ii}^3 \tag{65}$$

m_i indicate the masses of the spheres. The entropy ($S = -\left(\partial F/\partial T\right)_\Omega$) of the hard sphere mixture, as in equation (51), can readily be derived from equation (59). Equation (60) can be used to obtain an expression for the concentration fluctuations, $S_{cc}(0)$, for binary hard sphere mixtures, i.e.

$$S_{cc}(0) = RT\left(\frac{\partial^2 G_{hs}}{\partial c^2}\right)_{T,p}^{-1} \tag{66}$$

Substitution of equations (60)-(65) in (66) gives (see Osman and Singh 1993, 1995):

$$S_{cc}^{hs}(0)^{-1} = \frac{1}{c_Ac_B} + \frac{\pi}{2\Omega}\left[\frac{9X^3d_3^2}{(1-\eta)^4} + \frac{18X^2d_2d_3 + 4XYd_3^2}{(1-\eta)^3} + \frac{9Xd_2^2 + 4Yd_1d_2 + 4Xd_1d_3 + (\pi/18\Omega)d_3^2}{(1-\eta)^2} - \right. \tag{67}$$

where

$$d_1 = \sigma_{AA} - \sigma_{BB}, d_2 = \sigma_{AA}^2 - \sigma_{BB}^2, d_3 = \sigma_{AA}^3 - \sigma_{BB}^3 \tag{68}$$

It is evident from equation (67) that if

$$\sigma_{AA} = \sigma_{BB} = \sigma_{AB} \tag{69}$$

then

$$S_{cc}^{hs}(0) = c_A c_A \tag{70}$$

Equation (69) is the required condition that a mixture of hard spheres is an ideal mixture.

The values of $S_{cc}^{*}(0)[= S_{cc}^{hs}(0)/c_A c_B]$ acquired from equation (67) for different values of size ratio, $\gamma(= \sigma_{BB}/\sigma_{AA}, \sigma_{BB} > \sigma_{AA})$ is shown in figure 13. The curve for $\gamma = 1$, corresponds to the ideal mixture. With the expansion of size ratio, the values of $S_{cc}^{*}(0)$ decrease rapidly from the ideal value indicating an ordered state. The larger the values of γ , the more ordered a state is achieved in the mixture for $\gamma > 2.0$; a flat minimum is observed over a wide range of concentrations.
The results of figure 13 display that $S_{cc}^{*}(0)$ cannot be greater than 1 for any size effect. Hence a binary hard-sphere mixture within the working conditions of equations (57) and (58) is consistently stable, i.e. there is no segregation for any mismatch size ratio. This is a notable result since the work by Lebowitz and Rowlinson (1964), who indicated that the excess Gibbs energy for a binary mixture is consistently negative for all size effects and so phase separation does not arise.

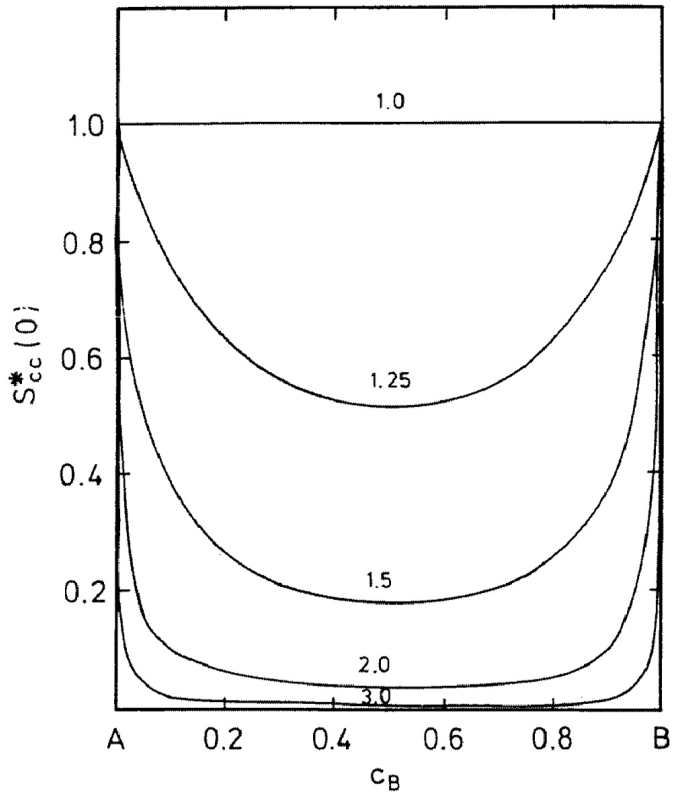

Figure 13: The reduced $S^*_{cc}(0)$ against composition of a binary hard sphere liquid mixture for different size ratio, $\gamma = 1.0$, 1.25, 1.5, 2.0 and 3.0 (after Osman and Singh (1995)).

6.2 Hard spheres beyond the Percus–Yevick approximation

Biben and Hansen (1991) evaluated the numerical solution of the integral equations associating the total (h_{ij}) and the direct (C_{ij}) correlation functions. In the Percus–Yevick approximation, one maintains

$$g_{ij}^{PY}(r) = \theta(r - \sigma_{ij})(1 + \gamma_{ij}(r)) \tag{71}$$

where

$$\gamma_{ij}(r) = h_{ij}(r) - C_{ij}(r) \tag{72}$$

$\theta(x)$ represents the step function. These authors utilized a parametrized form of equation (71) (for example, Baltone et al (BPGG) (1986), Rogers and Young (RY) (1984)),

$$g_{ij}^{BPGG}(r) = \theta(r - \sigma_{ij}) exp[(1 + s\gamma_{ij}(r))^{1/s} - 1] \tag{73}$$

$$g_{ij}^{RY}(r) = \theta(r - \sigma_{ij}) \left[1 + \frac{exp(\gamma_{ij}(r) f_{ij}(r)) - 1}{f_{ij}(r)}\right] \tag{74}$$

The parameters s and $f_{ij}(r)$ are modified to fulfill a thermodynamic consistency via the equation of state. The numerical solutions of equations (71)-(74) were obtained for different size ratios $y(= \sigma_A/\sigma_B)$, here $\sigma_A > \sigma_B$ = 0.5, 0.2, 0.15 and 0.1.

The results obtained for $\Lambda = c_A c_B S_{cc}(0)^{-1}$ are shown in figure 14 as a function of the packing fraction $\eta_2(\eta_2 = \pi\sigma_B^3/6\Omega_B$, is the partial packing fraction of the bigger component B). The results display that the mixture with the size ratio y = 0.5 conducts nearly ideally and the predictions of the PY, RY and BPGG equations are close for all η_2. These equations, ultimately, were discovered to differ extensively for larger y. $\Lambda(= c_A c_B S_{cc}(0)^{-1})$ received with the PY closure continuously increases with η_2 , whereas RY and PBGG closures indicate an opposite movement. With enriching η_2 ,Λ falls rapidly, i.e. the concentration fluctuations become very strong. On its distinction, these authors finalize that phase separation occurs for size ratios $y \geq 2$.

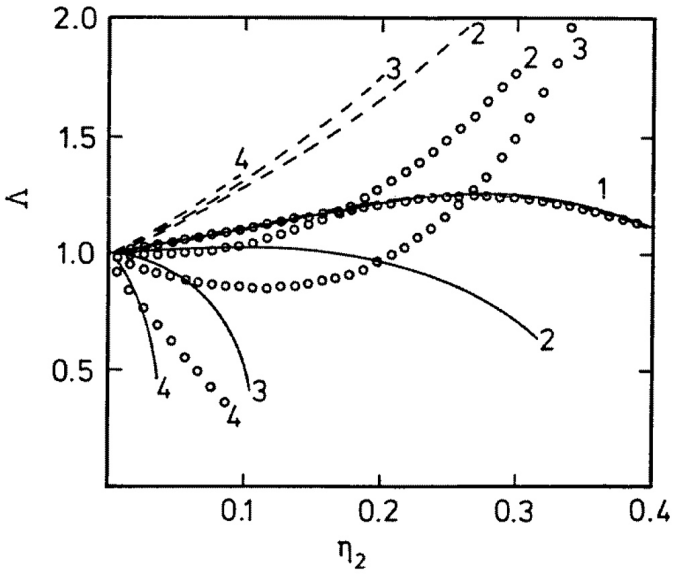

Figure 14: Concentration fluctuations $\Lambda = c_A c_B S_{cc}(0)^{-1}$ against packing fraction η_2.Full curves,unsteady curves and circles are for the RY, PY and BPGG results, respectively. Curves labelled from 1 to 4 are for size ratio y = 0.5, 0.2, 0.15 and 0.1 (y = σ_A/σ_B, $\sigma_A > \sigma_B$ after Biben and Hansen (1991)).

Quite descending in line, Lekkerkerker and Stroobants (1993) analyzed the osmotic pressure of a mixture of hard-sphere colloids with strongly asymmetric sizes. The osmotic equation of state expresses a spinodal instability. The origin of the instability is interpreted to be the attractive depletion interaction between the large spheres, which is caused by the presence of the smaller spheres.
Furthermore, Frenkel and Louis (1992) in an attempt to map hard-core mixtures onto lattice models with nearest-neighbor attraction, verified that the entropy associated with hard-core repulsion may pose as an effective attraction that causes the demixing process. Dijkstra and Frenkel (1994) performed grand canonical Monte Carlo simulation studies of a mixture consisting of large and small cubes where the independent variables were the fugacities of the cubes. Such a method also generates a demixing transition in a binary hard-core mixture.

7 Summary

Deviations in the equilibrium surface composition of ordered alloys with temperature depend on interatomic energetic parameters, the surface orientation, and its primary, low-temperature termination. In case the segregation process is endothermic and the low-temperature termination corresponds to entropy-driven segregation that grows with temperature is expected. The segregation properties of liquid binary alloys are systematically investigated via two different thermodynamic quantities, namely, the energy of mixing ΔF and the entropy of mixing ΔS. Both ΔF and ΔS agree with the interrelated experimental data in the mixed state.We are now in a situation to draw the following summary of this project (i) The GMT together with the perturbation approach can explain, at least qualitatively, the energy of mixing and the thermodynamic state-dependent partial miscibility of liquid binary alloys. (ii) Below the critical temperature, this alloy starts getting partially miscible. The critical concentration matches precisely with the experimental value of Predel . (iii) Finding positiveness of the energy of mixing would have been impossible if the volume dependent term, ΔF vol was not there as a prevalent positive quantity.

References

[1] Krzysztof Fitzner. An extension of krupkowski's method of interpreting thermodynamic properties of multicomponent compound-forming alloys. *Calphad*, 5(4):239–253, 1981.

[2] Uresh Vahalia, Peter Dowben, and Allen Miller. Surface segregation in binary alloys. *Journal of Vacuum Science & Technology A: Vacuum, Surfaces, and Films*, 4(3):1675–1679, 1986.

[3] RN Singh and F Sommer. Segregation and immiscibility in liquid binary alloys. *Reports on Progress in physics*, 60(1):57, 1997.

[4] Ralph Hultgren, Pramod D Desai, Donald T Hawkins, Molly Gleiser, and Kenneth K Kelley. Selected values of the thermodynamic properties of binary alloys. Technical report, National Standard Reference Data System, 1973.

[5] GV Raynor and W Hume-Rothery. The structure of metals and alloys. *Institute of Metals, London*, page 60, 1954.

[6] HL Lukas and SG Fries. Demonstration of the use of "bingss" with the mg-zn system as example. *Journal of phase Equilibria*, 13(5):532–542, 1992.

[7] Bruno Predel and Hartmut Sandig. Thermodynamische untersuchungen der systeme aluminium-wismut, aluminium-indium und kupfer-thallium. *Materials Science and Engineering*, 4(1):49–57, 1969.

[8] Hiroshi Ohtani, Seiichi Ono, Kodai Doi, and Mitsuhiro HASEBE. Phd thesis, university of provence, marseille, france phd thesis, university of provence, marseille, france, 1985. *Materials transactions*, 45(3):614–624, 2004.